YEARLY TECHNICAL PROGRESS REPORT

submitted to

U. S. Department of Energy

Reporting Periods: 09/2702 – 09/26/03

December 26, 2003

Title: **Intelligent Monitoring System With High Temperature Distributed Fiberoptic Sensor For Power Plant Combustion Processes**

Authors: **Kwang Y. Lee, Stuart S. Yin, Andre Boheman**

The Pennsylvania State University
Department of Electrical Engineering
University Park, PA 16802
Ph. (814) 865-2621, Fax (814) 865-7065
kwanglee@psu.edu

Grant Number: DE-FG26-02NT41532
Performance Period: 09/27/2002 to 09/26/2005

DISCLAIMER

ABSTRACT

The objective of the proposed work is to develop an intelligent distributed fiber optical sensor system for real-time monitoring of high temperature in a boiler furnace in power plants. Of particular interest is the estimation of spatial and temporal distributions of high temperatures within a boiler furnace, which will be essential in assessing and controlling the mechanisms that form and remove pollutants at the source, such as NOx. The basic approach in developing the proposed sensor system is three fold: (1) development of high temperature distributed fiber optical sensor capable of measuring temperatures greater than 2000 C degree with spatial resolution of less than 1 cm; (2) development of distributed parameter system (DPS) models to map the three-dimensional (3D) temperature distribution for the furnace; and (3) development of an intelligent monitoring system for real-time monitoring of the 3D boiler temperature distribution.

Under Task 1, the efforts focused on developing an innovative high temperature distributed fiber optic sensor by fabricating in-fiber gratings in single crystal sapphire fibers. So far, our major accomplishments include: Successfully grown alumina cladding layers on single crystal sapphire fibers, successfully fabricated in-fiber gratings in single crystal sapphire fibers, and successfully developed a high temperature distributed fiber optic sensor. Under Task 2, the emphasis has been on putting into place a computational capability for simulation of combustors. A PC workstation was acquired with dual Xeon processors and sufficient memory to support 3-D calculations. An existing license for Fluent software was expanded to include two PC processes, where the existing license was for a Unix workstation. Under Task 3, intelligent state estimation theory is being developed which will map the set of 1D (located judiciously within a 3D environment) measurement data into a 3D temperature profile. This theory presents a semigroup-based approach to the design and training of a system type neural network which performs function extrapolation. The assumption of the semigroup property suffices to guarantee the existence of a generic mathematical architecture and operation which is explicit enough to support the direct design and training of a neural network.

TABLE OF CONTENTS

TECHNICAL PROGRESS REPORT

TECHNICAL PROGRESS REPORT

December 26, 2003

Title: **Intelligent Monitoring System With High Temperature Distributed Fiberoptic Sensor For Power Plant Combustion Processes**

Authors: Kwang Y. Lee, Stuart S. Yin, Andre Boheman
Students: J.A. Chavez, S.H. Nam, C. Zhan, Melanie Fox, B.H. Kim, John Valas
The Pennsylvania State University
Department of Electrical Engineering
University Park, PA 16802
Ph. (814) 865-2621, Fax (814) 865-7065
kwanglee@psu.edu
Grant Number: DE-FG26-02NT41532
Performance Period: 09/27/2002 to 09/26/2005

OVERVIEW AND PROGRESS TO DATE

The objective of the proposed work is to develop an intelligent distributed fiber optical sensor system for real-time monitoring of high temperature in a boiler furnace in power plants. Of particular interest is the estimation of spatial and temporal distributions of high temperatures within a boiler furnace, which will be essential in assessing and controlling the mechanisms that form and remove pollutants at the source, such as NOx.

The basic approach in developing the proposed sensor system is three fold: (1) development of high temperature distributed fiber optical sensor capable of measuring temperatures greater than 2000 C degree with spatial resolution of less than 1 cm; (2) development of distributed parameter system (DPS) models to map the three-dimensional (3D) temperature distribution for the furnace; and (3) development of an intelligent monitoring system for real-time monitoring of the 3D boiler temperature distribution.

TASK 1. FIBEROPTIC SENSOR DEVELOPMENT

1.1 Objectives and Motivations

The objective of this task is to develop an innovative high temperature distributed fiber optic sensor by fabricating in-fiber gratings in single crystal sapphire fibers. This unique high temperature distributed fiber optic sensor can precisely monitor the temperature distribution inside a boiler, which, in turn, could substantially increase the burning efficiency and reduce the pollution emission (e.g., NO_x). Figures 1(a) and 1(b) illustrate a power plant and a boiler with embedded fiber optic sensors.

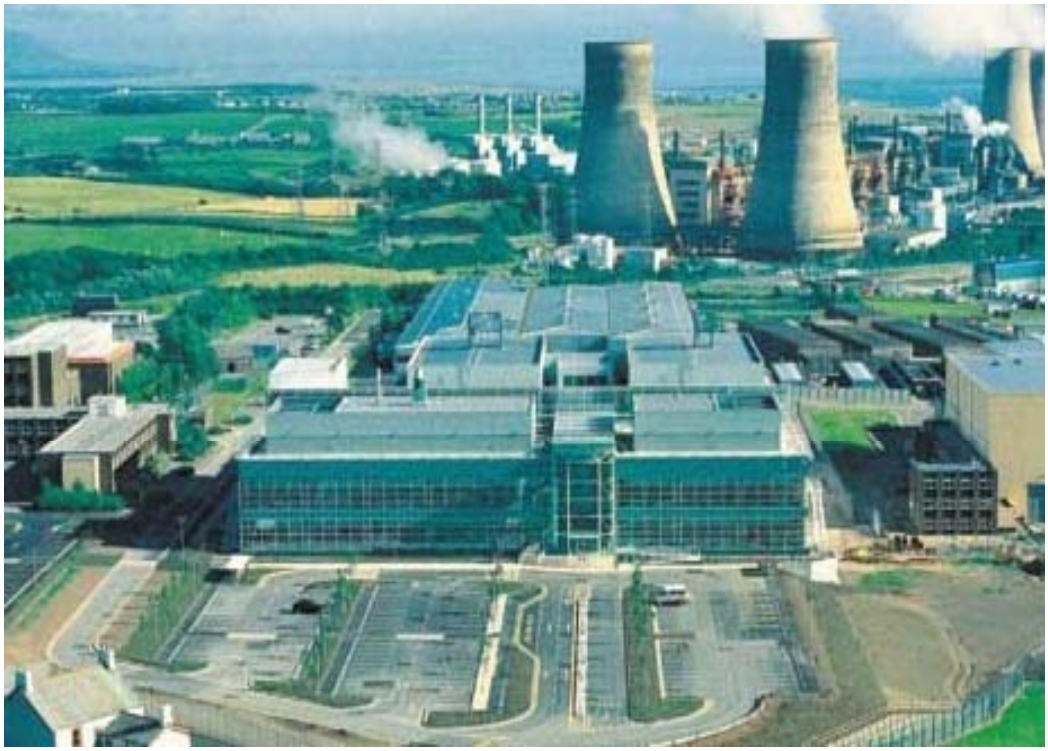

Fig. 1.(a) A picture of a power plant

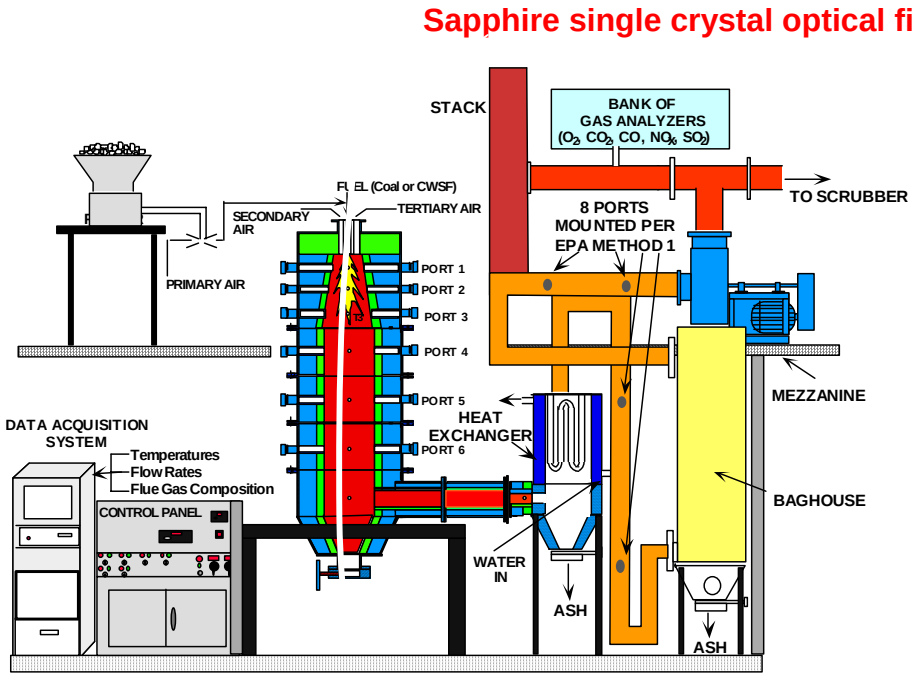

Fig. 1. (b) A boiler with embedded fiber optic sensor.

A Ph.D. student with the support from a couple of master students under Prof. S. Yin's supervision began work on this project since project took off in October, 2002. The project is well on track. We finished all the proposed tasks within the schedule. A detailed description on accomplishment is given in Section 1.2.

1.2 Major Accomplishments

1.2.1 Fabricate alumina cladding layers on single crystal sapphire fibers.

To fabricate alumina cladding layer in a single crystal sapphire fiber, 11 nm alumina nano-particles with 99.99% purity were deposited and densified on the sapphire fiber core. The method used to attach the alumina particles involved the use of an acrylic acid monomer, a polymetric initiator consisting of benzoyl peroxide, an accelerator of DMPT (N, N-Dimethyl-p-Toluidine) , and distilled water as a stabilizer. The basic fabrication process can be summarized as follows:

- The fiber samples are cleaned by hydrochloric acid (1 mL/1 cm^3) and are then rinsed twice with distilled water that has been double boiled for purification. After rinsing the fiber, its ends are capped with PTFE or FEP buffers and immersed in the distilled water until the polymer is prepared.

- The preparation of the polymer is a little bit time-consuming task by which nano-powders must first be dispersed. In our case, both $\alpha-$ and $\gamma-$ alumina (Al_2O_3) powders have been used; and they are equally dispersed with ethanol. The $\gamma-Al_2O_3$ was composed of 11 nm particles with 99.99% purity; while the $\alpha-Al_2O_3$ had particle sizes of 27-43 nm and a purity of 99.5%. Needless to say for this sensor to properly operate as a 2000 ^oC sensor, the final alumina particles chosen should be as small as possible in order to avoid loss of transmission due to the grain boundaries; and the purity must be as high as possible otherwise the operating point of the alumina (prior to melting or softening) is lowered in temperature. It is found that 99.5% alumina is only effective for temperatures below about 1600 ^oC ; while the 99.9% purity will be acceptable in greater than 1900 ^oC temperatures.

- With those decisions in mind the alumina is then dispersed in ethanol (10 mL/g) and ultrasonically stirred for a minimum of two hours and preferably until dry. The necessary weights are all based upon the weight of the monomer and are as follows: 20% must be alumina, 0.5 to 2% of benzoyl peroxide, 0.5 to 2% of DMPT, and 100% of both distilled water and acrylic acid.

- Once the amounts have been measured, two precipitate powders are combined and grained as fine as possible. The distilled water is then drop-wise combined to avoid any major reactions; and likewise, the acrylic acid is drop-wise combined. The resultant mixture is then ultrasonically mixed for a minimum of two hours. After that time, the temperature is critical and must be measured to verify it is at room temperature. If it is not, it should be allowed to cool while on top of a stirrer; otherwise, the accelerator will

harden the overall suspension too quickly to determine the proper time to maintain the sapphire fiber core immersed.

- Once at room temperature, DMPT is added drop-wise, hand stirred for two minutes, and the fiber sample with end caps is immersed for 30 to 45 minutes depending on how well the suspension was hand stirred. Since the alumina seems to settle during this polymerization step, it is better to maintain the fiber laying flat on the bottom surface and not standing on one end. Thus that is the reason for the two end caps – to slightly suspend the fiber' surface from the crucible or beaker's bottom. After the allotted time, the fiber is then pulled as slow as possible from the suspension so as to maintain a uniform polymer coating on the core. At this point, the PTFE/FEP caps usually slide off the core since the fiber is pulled at an angle; therefore, the two end caps are replaced and the fiber is allowed to polymerize for a period of no less than 24 hours. Once the polymer has set, its blinder must be removed by pre-firing at 600 ^{o}C for one hour. Care must be taken to avoid burning of the polymer. Thus, it is essential to increase temperature at no more than 3 ^{o}C/minute, and preferably at 2 ^{o}C/minute. After this pre-firing stage, there does not seem to be much difference between allowing fiber samples to cool to room temperature or to simultaneously perform the secondary firing stage. Either way, the ramping rate should be approximately 5 ^{o}C/minute until reaching the ideal sintering temperature of the alumina powder. In most cases, a temperature of 1600 ^{o}C is sufficient in an air atmosphere; and maintaining this temperature for three hours produces a quite dense coating around the fiber. The cool-down cycle is critical importance as well. It is recommended that the rate be 5 ^{o}C/minute; though, cracks could be avoided at 10 ^{o}C/minute also. Once this procedure is complete, a stable thick layer of cladding can be built by repeating every step with the exception of the hydrochloric cleaning of the sapphire sample.

Figure 2 shows a single crystal sapphire fiber with alumina cladding. The diameter of the sapphire fiber is 150 microns, and the thickness of the cladding layer is around 2 microns. Thicker cladding layer can be obtained by repeating above fabrication process via multiple layer coating.

1.2.2 Fabricate in-fiber corrugated long period gratings in single crystal sapphire fibers.

To achieve distributed fiber optic sensing capability, we have to fabricate in fiber corrugated long period gratings. Since sapphire is a very strong material, gratings cannot be written in traditional approaches such as using UV light. To realize this goal, we investigated several approaches and the best one would be used for the final product fabrication, as described in the following.

1.2.2.1 Fabricate in-fiber long period grating in single crystal sapphire fiber by etching.

The process began by first obtaining a sapphire fiber from Photran LLC. The fiber provided had a 150 μm diameter core and was approximately ½ meter in length. Figure 3 summarizes the fabrication process.

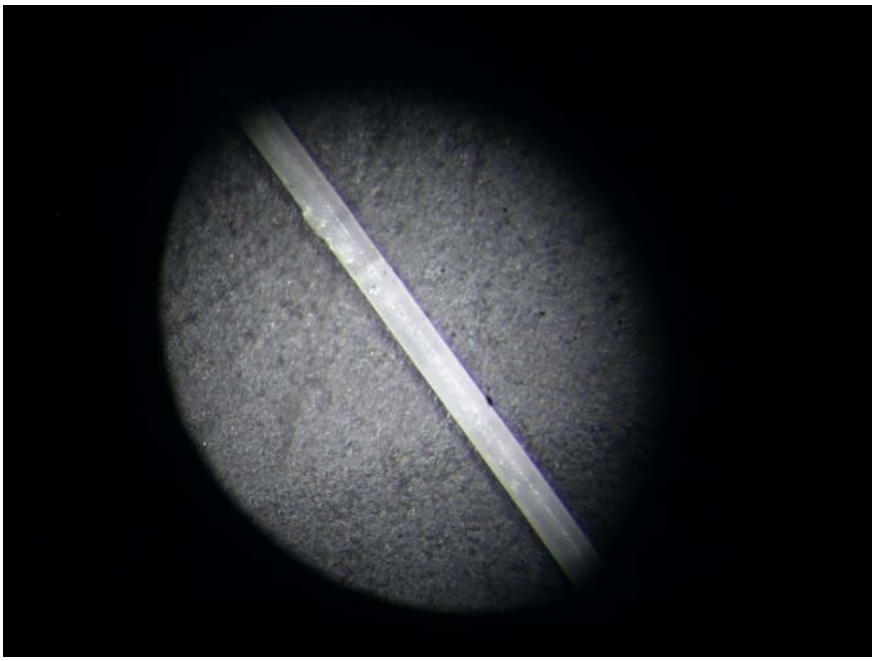

Figure 2 A single crystal sapphire fiber with alumina cladding. The diameter of sapphire core is 150 microns and the thickness of the cladding layer is around 2 microns.

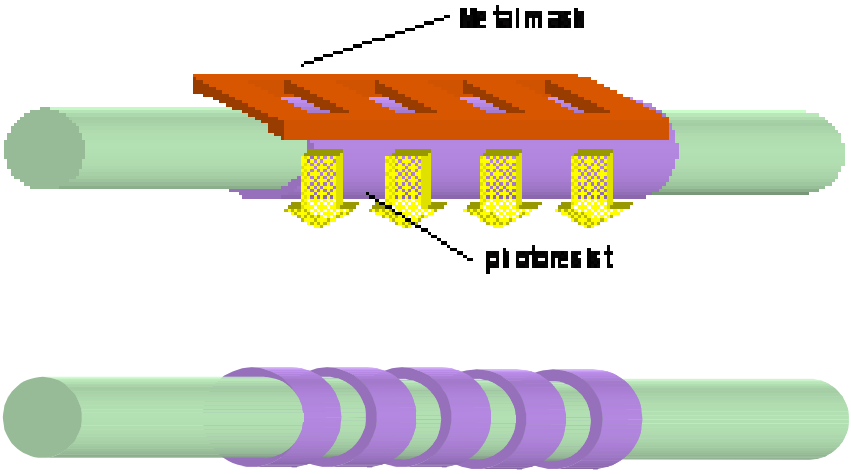

Fig. 3 An illustration of process of fabricating in-fiber grating in single crystal sapphire fiber.

The fiber was first coated by positive photoresist with a period of 300 μm, as shown in Fig. 4(a). The fiber was then placed in a sputtering system and a 100 $\mathring{A}$ chromium layer was deposited and

followed by 1500 Å of gold, as shown in Fig. 4(b). After that, this fiber was chemically etched with a sulfuric and phosphoric acid (H_3PO_4) solution at around 350 ^oC. Since gold is an inactive material, the portion with gold coating will not be etched as fast as the areas without the gold coating. Thus, periodic grating structure can be obtained. The major advantages of this approach are:

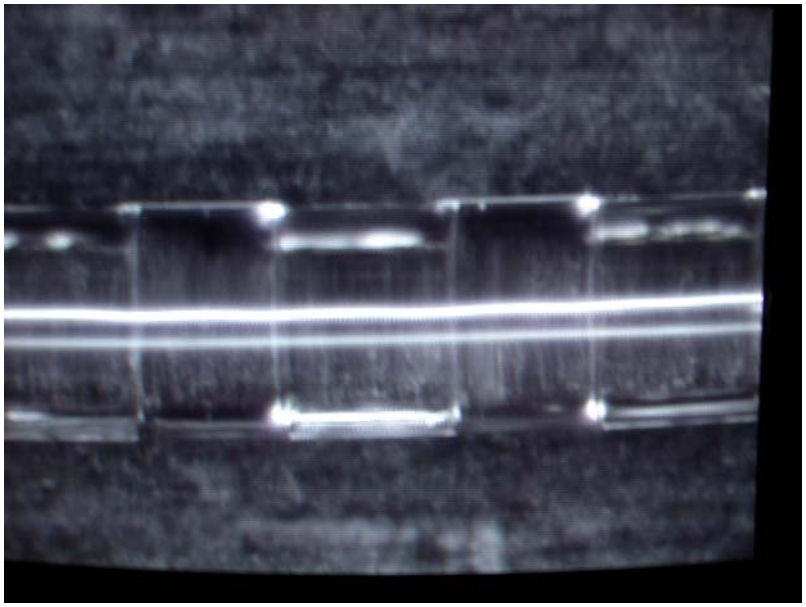

(a)

(b)

Figure 4 (a) Single crystal sapphire fiber with periodic coated photoresist layer; (b) single crystal sapphire fiber with periodic coated gold layer.

- The grating dimension and structure can be precisely controlled.

However, since the etching process is slow and the gold protective coating will also be etched eventually, it is difficult to fabricate grating with large depth.

1.2.2.2 Fabricate in-fiber long period grating in single crystal sapphire fiber by dicing.

To fabricate in-fiber grating with large depth, we also used dicing approach. In the experiment, a 5 cm long single crystal sapphire fiber, with 150 micron diameter, was used. In order to hold the fiber, the fiber sample was attached to a 2" x 2" glass substrate with Crystalbond 509 adhesive and the use of a hot plate at 135 ^{o}C. The glass substrate was then placed on a computer-controlled chuck underneath a diamond saw blade. By applying a minimum vacuum of 80 psi, the substrate was firmly held by the chuck once it was properly aligned. The control box was then programmed to provide continuous cuts with a period of 500 micron and a depth of 50 micron. Note that, the thickness of diamond blade is about 250 micron so that a 50% duty cycle grating can be obtained. Figure 5 shows the fabricated grating using dicing approach. As aforementioned, the major advantages of this approach are:

- Large depth grating can be fabricated.
- Simple and fast speed.

However, it also has following limitations:

- The minimum grating period is limited by the thickness of diamond saw blade.
- It is difficult to fabricate complicated micro structures.

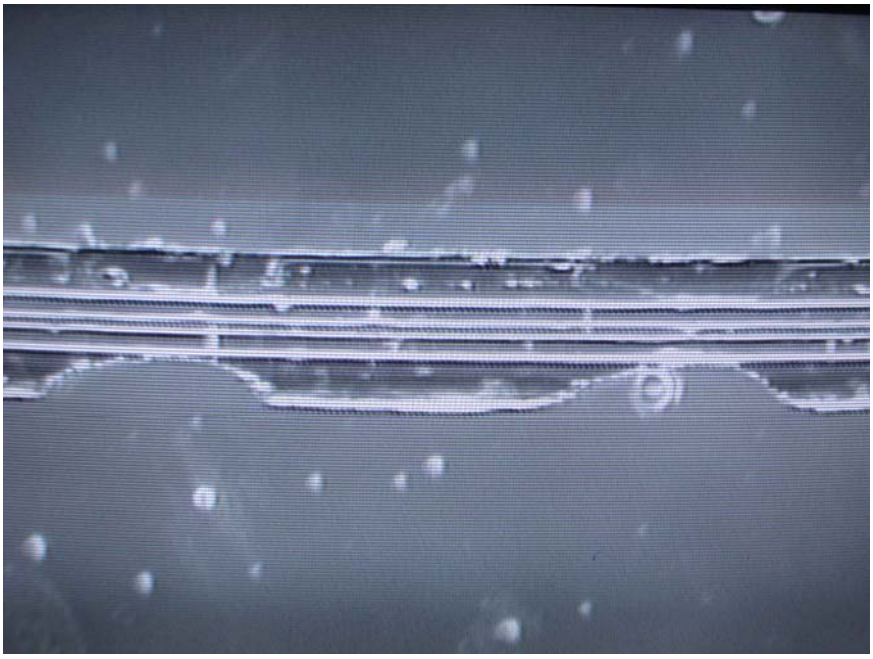

Fig. 5 Fabricate in-fiber long period grating in single crystal sapphire fiber by precise dicing.

1.2.3 Investigate distributed fiber optic sensing using single crystal sapphire fiber.

In this project period, we also investigated distributed fiber optic sensing using single crystal sapphire fiber.

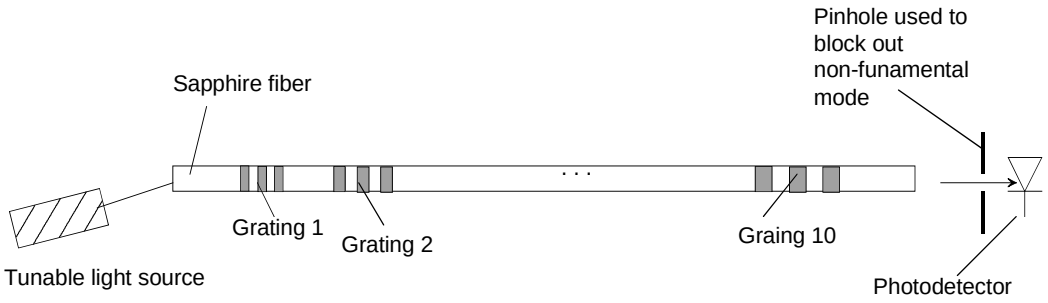

Figure 6. An illustration of working principle of high temperature distributed fiber optic sensor in single crystal sapphire fiber.

Due to the existence of long period grating, there is a mode coupling between core and cladding modes, as mathematically given by

$$\lambda_p = (n_{co} - n_{cl})\Lambda, \qquad (1)$$

where λ_p represents the resonant wavelength, n_{co} and n_{cl} represent the effective core and cladding refractive index, respectively, and Λ denotes the grating period. When there is a temperature change, both the effective refractive indices and the grating period will also change due to the thermal-optic and thermal expansion effects. Thus, the resonant wavelength will be a function of temperature, by which temperature sensing can be performed. By fabricating a set of gratings with different central resonant wavelengths, distributed fiber optic sensing can be achieved, as shown in Fig. 6. We stress that since single crystal sapphire fiber has a very high melting temperature (> 2000 ^{o}C), high temperature sensing can be achieved.

1.3 Future Work Plan

In the next year, we will implement the project according to the working plan as described in the original proposal, specifically as follows:

- Continue fabricating in fiber gratings in single crystal sapphire fiber with better performance and quality.
- Apply the fabricated unique grating to high temperature distributed fiber optic sensing.

TASK 2: BOILER FURNACE MONITORING MODEL DEVELOPMENT

Development of the multi-dimensional combustion simulation model has been the focus of activities by Prof. Boehman and his student. The effort has primarily been to get a functional workstation, with CFD software, into place and to train the student on its application to multi-dimensional combustion simulation.

The workstation acquired for this project comprises dual-Xeon 2.0 GHz processors and 512 MB RAM. A one-year license for FLUENT 6.1 has been obtained. The graduate student has been training to learn FLUENT to achieve the goals of this project with regard to multi-dimensional simulation.

The graduate student is now working with a 2-D model of the Down Fired Combustor Modeling this boiler has provided the graduate student the opportunity to become skilled using FLUENT, to leverage existing grids and extensive prior experimental work for comparison. This represents a shift from the initial direction, which was to work on a 3-D simulation of the Demonstration Boiler. Subsequent applications of FLUENT will extend to the Drop Tube Reactor (DTR) and the Demonstration Boiler.

The student has become proficient at using Gambit 2.1.6, the grid generation software for FLUENT, in preparing the demonstration boiler grid for simulation. Specific skills include:

- discretizing grid volumes
- meshing complex geometries
- evaluating grid for skewness
- grid refinement
- creating mesh for data collection at desired spatial positions

The student has also acquired skills in FLUENT, specifically:

- prePDF generation (for combustion simulations)
- solver selection
- premixed & non-premixed systems
- steady state or transient simulations
- air-staging
- knowledge to carry out validation studies

TASK 3. INTELLIGENT MONITORING SYSTEM DEVELOPMENT

3.1 Objectives and Motivations

For applications to control systems, estimation techniques are often required to compensate for an inadequate amount of data, arising from the unavailability of that data. In the past, for systems described by ordinary differential equations, various estimation techniques have been developed with the most popular (and successful) ones being based on variations of the Kalman filtering theory. However, as control theory has been expanded to include more complex behavior, such as distributed parameter systems, described by partial differential equations, the estimation

problem has taken on a new importance, because now it is necessary to provide estimated data at a great (theoretically infinite) number of points. A need therefore exists for a generalized estimation technique which can be applied to a broad class of nonlinear systems, any one of whose behavior is described by a partial differential equation. Stated very concisely, a need exists for a technique which can begin with a set of data derived from a few discrete points within some continuum in one, two or three dimensional space and which can then develop estimated data at as many points as needed within the continuum, in a manner which is dynamically consistent with the empirical data points, and additionally, to extrapolate the resulting function into an adjoining region of space for which there is no data. The purpose of the present research is to illustrate the development of a technique for estimating the temperatures at all interior points of a furnace, given only the temperatures at a few discrete points within one portion of the furnace (for example, within the first three-fourths of the axial span of the furnace). The significance of the application lies in the fact that the actual boiler furnace involves dynamics of great complexity, with both nonlinearities and time varying characteristics, combined with significant uncertainties in model parameters. The complete system for providing the needed estimation will be referred to as an intelligent monitoring system, because the basis for its development involves the use of intelligent techniques.

Ph.D. students under Prof. Kwang. Lee's supervision began work on this project since project took off in October, 2002. The project is well on track. We finished all the proposed tasks within the schedule.

3.2 Development of Intelligent Monitoring System

Since the monitoring system will be applied to the estimation of temperatures inside a boiler furnace, from this point on, the description of the technique will be tailored to the given problem. The problem can be formulated as follows. Given a set of empirical (temperature) data derived from a finite number of points within one section of the 3-dimensional continuum defined by the furnace interior, develop a continuum system model for the temperature at all interior points of the furnace, including those sections for which there is no data. It is assumed throughout that there is no (prior) analytic expression for the given data or for the ultimate continuum model. The technique for performing system modeling is hinged on developing a specific type of model, namely one that possesses a semigroup property. In this case, because of the axial symmetry of the furnace, a model is sought which can be expressed as $T(z,r) = C^T(z)E(r)$, where the product is to be interpreted as a vector product, and where $E(r)$ functions as an orthonormal finite-dimensional basis, and where $C(z)$ is a coefficient vector which satisfies the semigroup property: $C[z] = \Phi[z] \cdot C[0]$, where $\Phi(z_1 + z_2) = \Phi(z_1) \cdot \Phi(z_2)$.

At its highest level, the technique for developing the model can be described as follows. Assume that the axis of the furnace is aligned with the z-axis and that there are N temperature probes, spaced equidistantly along the z-axis from top to bottom, and that each probe supplies M temperature readings, at radially-equidistant points from the axis of the cylinder to the wall of the cylinder. The procedure begins by reorganizing the data into an indexed family of N functions $\{T_{z=1}(r), T_{z=2}(r), \cdots, T_{z=N}(r)\}$, where for any index $z = z_i$, there are M (radial) temperature values. (Each member function originates with one probe and each member function is called a spline.) Next, a (trial and error) search is conducted for small set of n ($n \ll N$, $n < M$)

maximally linearly independent functions (splines) from within the family of splines. Once found, the set of *n* linearly independent functions is converted into an orthonomal basis set. Then, for each spline, that particular linear combination of the basis set which provides the best least squares approximation to the given empirical data at that spline is found. For each spline z_i, the computed linear combination becomes the coefficient vector for that spline $C[z_i]$. The orthonomal basis is referred to as $E(r)$ and the complete set of linear combinations becomes the coefficient vector $C(z)$. $C(z)$ must ultimately have the semi-group property: $C[z] = \Phi[z] \cdot C[0]$, where $\Phi(z_1 + z_2) = \Phi(z_1) \cdot \Phi(z_2)$. Because no analytic expression is available for either the composite system or the individual splines, neural networks are used to develop the model. However, unlike conventional neural network architectures which would attempt to implement the mapping as a single R^2 to R^1, this approach follows semigroup theory which suggests that this particular mapping should be implemented as two mappings, requiring two cooperating channels of neural networks as shown in Fig. 1. The Function channel implements the *n* dimensional function space spanned by the *n* basis vectors *E(r);* the semigroup channel provides a coefficient vector (dependent on *z*) to the Function channel to determine a specific function from within the function space.

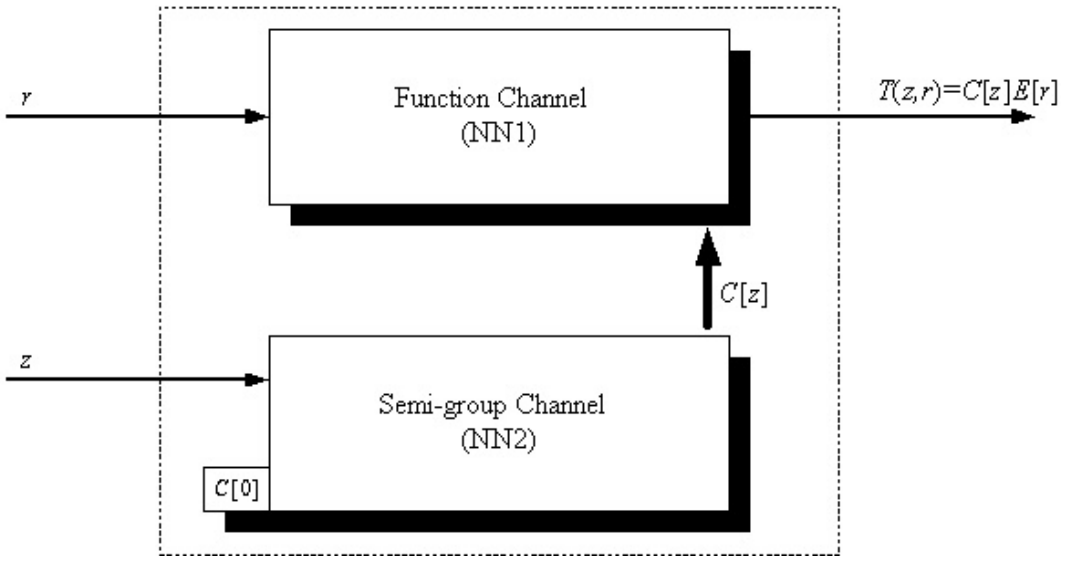

Fig.1. System Architecture.

There are roughly three parts to the technique. First, referred to as algebraic decomposition, only the Function channel is used. The basis set of vectors is defined and a preliminary coefficient vector is formed. Second, referred to as smoothing, only the semigroup channel is used. The objective is to smoothen the preliminary coefficient vector into a final coefficient vector. Third, extrapolation is performed on $C(z)$ to "stretch" it to span the region of furnace space for which there is no data. Finally, analytic expressions are obtained for each component of the basis set and for each component of the coefficient vector, and the (continuum) model is then obtained by performing the vector expansion indicated in the expression: $T(z,r) = C^T(z)E(r)$.

3.2.1 Design of Function channel (RBF network).

The function channel consists of *n* Radial Basis Function (RBF) networks, each one of which implements one orthonomal vector of an *n*-dimensional basis set of vectors. The outputs of the orthonomal vectors are linearly summed so that the channel spans an n-dimensional function space. Fig. 2 shows the inside of system architecture. In this research, *n* has been tailored to $n = 2$.

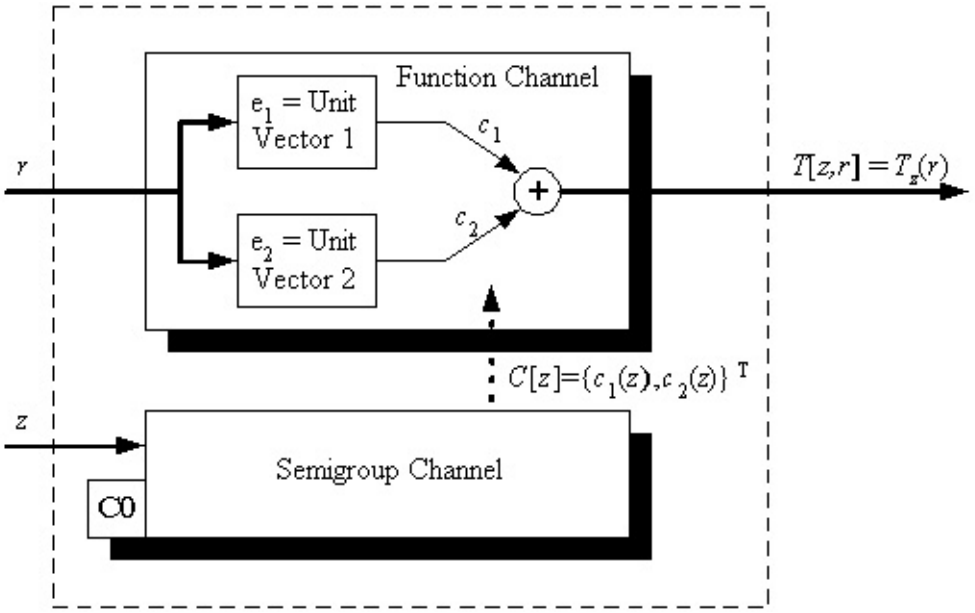

Fig. 2. Semigroup-based neural network architecture.

The RBF network is designed rather than trained, where the design is based on algebraic decomposition. Fig. 3 shows the procedure for determining linearly independent set. A more detailed description is as follows:

Step 1. Choose a set of *n* maximally linearly independent functions from the given set $\{T_{z=1}(r), T_{z=2}(r), \cdots, T_{z=N}(r)\}$ of empirical data functions. Refer to Fig. 3. (NOTE: For clarity, the remaining steps assume that the algebraic dimensionality is $n = 2$, and that the basis set chosen is: $\{T_{z=5}(r),\ T_{z=16}(r)\}$. For clarity, these are referred to as $\{V_1,\ V_2\}$.

Step 2. Convert the basis set $\{V_1,\ V_2\}$ into an orthonormal set $\{\tilde{V}_1,\ \tilde{V}_2\}$.

Step 3. Using an RBF architecture, design (do not train) neural network $e_1(r)$ to function as $\tilde{V}_1$ and design neural network $e_2(r)$ to function as $\tilde{V}_2$.

Step 4. For each spline z_k, compute the coefficients $c_1(z_k)$ and $c_2(z_k)$ which result from the application of the following least-squares algorithm:

$$E_{zk} = \sum_{i=1}^{i=M} [T_{zk}(r_i) - \tilde{T}f_{zk}(r_i)]^2 = \sum_{i=1}^{i=M} [T_{zk}(r_i) - \{c_1(z_k)e_1(r_i) + c_2(z_k)e_2(r_i)\}]^2 \quad .$$

Step 5. At the conclusion of algebraic decomposition, there are (N) functions constructed $\left\{\tilde{T}_{z=1}(r), \tilde{T}_{z=2}(r), ..., \tilde{T}_{z=N}(r)\right\}$ and there are (N) coefficient vectors formed: $\{C[1], C[2], ..., C[N]\}$, where each vector has dimensionality 2, that is, $C[z] = \{c_1(z), c_2(z)\}^T$. The significance of the coefficient vector and basis vectors is that, for any one spline z: $\tilde{T}_z(r) = c_1(z)e_1(r) + c_2(z)e_2(r)$.

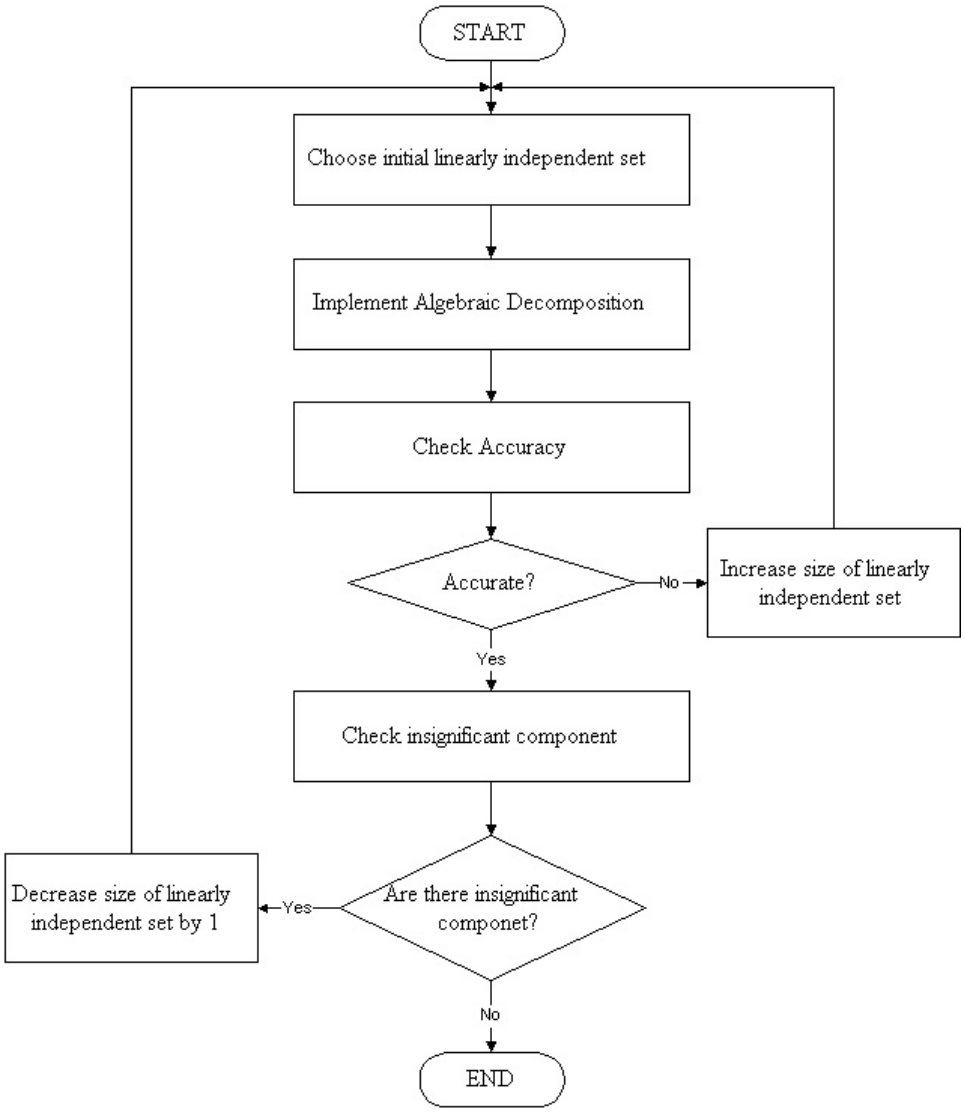

Fig.3. Procedure for determining linearly independent set.

3.2.2 Design and training for the semigroup channel.

The design of the Semigroup channel is an adaptation of the Elman architecture, in which the input is split into a dynamic scalar component z and a static vector component $C[0]$ and the output is a vector $C[z]$, where the dimensionality is determined by the previous algebraic decomposition process[1]. During training, the semi-group channel receives a preliminary coefficient vector $C[z]$ as input and produces a smoothened coefficient vector $\widetilde{C}[z]$. One

objective of training is to replicate the vector $C[z]$ with a vector $\widetilde{C}[z]$ which has the following semigroup property: $\widetilde{C}[z] = \Phi[z] \cdot \widetilde{C}[0]$, where $\Phi(z_1 + z_2) = \Phi(z_1) \cdot \Phi(z_2)$.

However, there is a secondary objective of training; the channel must also "replicate" the semigroup property of the trajectory by gradually acquiring a semigroup property of its own, in weight space (The existence of this acquired semigroup property becomes the basis for extrapolation.). In order to elicit this gradual acquisition of the semigroup property, it is necessary that the training in this second step (semigroup tracking) occurs in a graduated manner. That is, although it will not be illustrated as part of this report, the Elman network plays an additional important role in function extrapolation, which explains the need for this specialized (graduated) training technique. This gradual training technique consists of a series of trainings, where each training reinforces the previous training as follows. One training step corresponds to the network learning to replicate a given section of the overall coefficient trajectory. The next training step corresponds to the network learning to replicate the next incrementally increased trajectory. The last training step corresponds to the network learning to replicate the complete trajectory.

Extrapolation can only begin after a strong convergence has occurred in the Elman neural network weight space (refer to Fig. 4.) Specifically, the weights associated with W_{OUT}, W_{FB}, W_C must remain fixed and the weight changes associated with W_K must follow an easily discernible pattern. Extrapolation is then based on identifying the pattern and then continuing it. The role that the semigroup property plays in all of this is that the existence of the semigroup property ensures an easily detectable pattern.

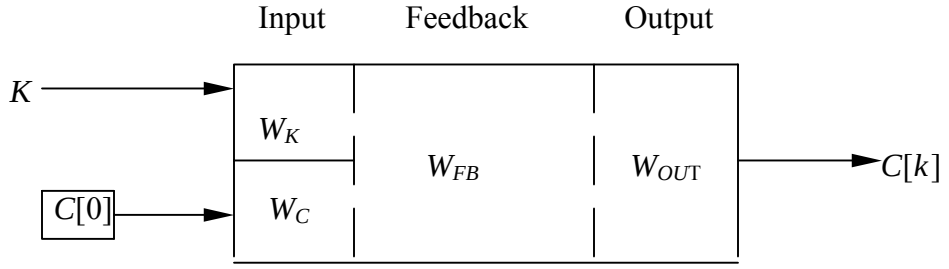

Fig.4. Allocation of weights in weight space.

3.3 Simulation and Estimation Results

3.3.1 Basic assumption for simulation.

For simulation purposes, the temperature data is simulated as follows. It is assumed that the furnace is cylindrical in shape, with a height of 13.3 meters and a radius (R) of 2 meters [2]. The internal dynamic behavior consists of a fluid-flow field, combined with a temperature field, which take place in laminar tube flow. There is an inlet section in which the velocity profile first forms and in which the complex thermodynamic phenomena associated with the jet flames takes place and the boundary layer equations have their most dominant effect. This is coupled directly to the main section in which the (parabolic) velocity profile is fully developed and remains

constant and in which the temperature profile develops and eventually remains constant. The following assumptions are made: constant wall temperature; forced convection – body forces are negligible; 2-D flow; steady-state conditions. The following are the assumed property values of the furnace model for generating the data: ρ = 0.368, c_p = 1150, U=velocity = 40 m/s, k = 0.0862.

Under these conditions, the solution for the temperature field becomes: $T - T_w \approx \frac{2\rho\, c_p U R^2}{k}\left[\frac{1}{4}\left(\frac{r}{R}\right)^2 - \frac{1}{16}\left(\frac{r}{R}\right)^4 - \frac{3}{16}\right]e^{-(0.1*z)}$. This is the function which is simulated. Furthermore, the following assumptions are made: there are 25 probes, each one at a fixed vertical position (given by z_i), and each one supplying 11 temperature readings which span the distance from the axis of the cylinder to the wall of the cylinder. Relative to the axis of the furnace, the probes span the first 10 meters of the furnace. (To demonstrate extrapolation, it is assumed that there is no data available for the last one-quarter of the furnace.)

To evaluate the performance of the proposed intelligent estimation technique, two situations are considered. First, we consider the case of a noise-free environment, so that the coefficient vector produced is smooth already. Second, we consider a noisy environment in which white gaussian noise (WGN) is added directly to the temperature field which then produces an unsmooth coefficient vector. In the latter case, we need to use the semi-group channel (Elman network) to smoothen the coefficient vector. Once the coefficient vector is smoothened, analytic expressions are obtained for each component of the basis vector set and for each component of the coefficient vector. Finally, the continuum temperature model is obtained by expanding the vector product: $T(z,r)=c_1[z]*e_1[r]+c_2[z]*e_2[r]$ using the derived component expressions.

3.3.2 Simulation Results.

3.3.2.1 Case I. (NOISE-FREE ENVIRONMENT)

We show the simulation results in Figs. 5 ~ 11. Fig. 5 and 6 show the coefficient vector components and Figs. 7 and 8 shows the basis vector components. Fig. 9 shows the empirical data and Fig. 10 shows the computed data which means the data from the calculation of the proposed intelligent technique. Fig. 11 shows the error between the two data sets and shows that the error between the computed data and the original empirical data at the sampled points is very small.

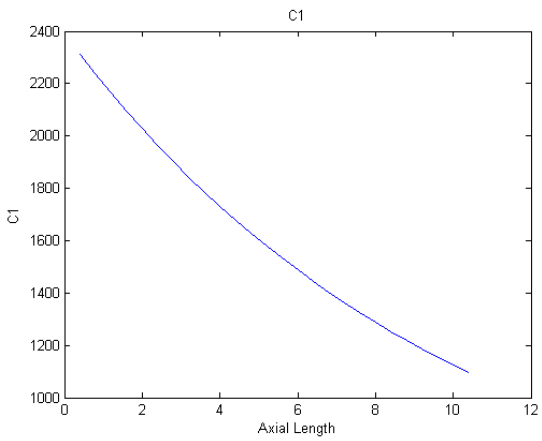

Fig. 5 . Coefficient Vector c_1.

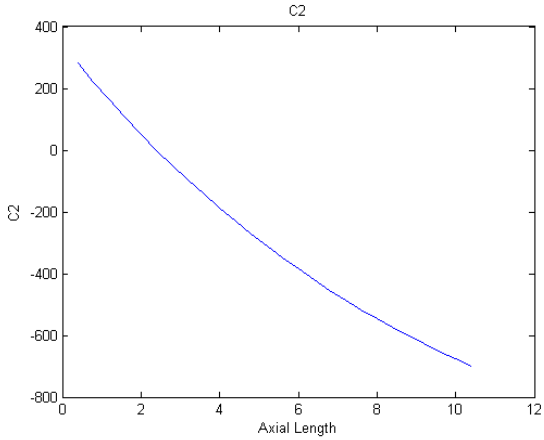

Fig. 6. Coefficient Vector c_2.

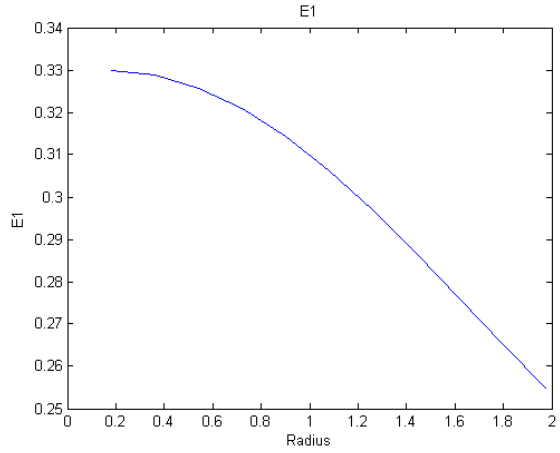

Fig. 7. Basis Vector e_1.

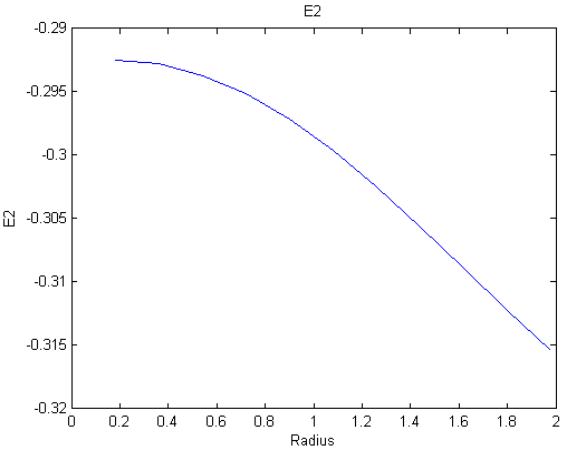

Fig. 8. Basis Vector e_2.

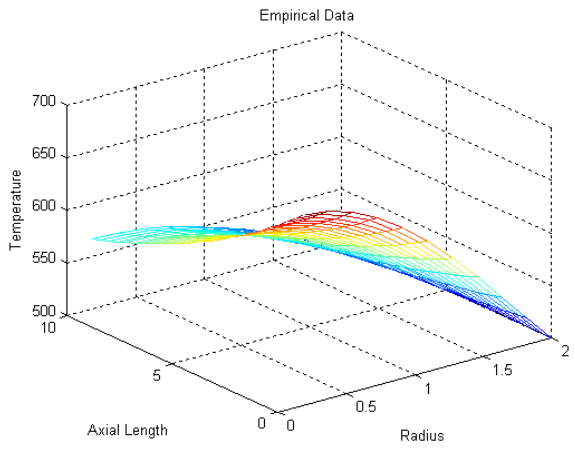

Fig. 9. Empirical Data.

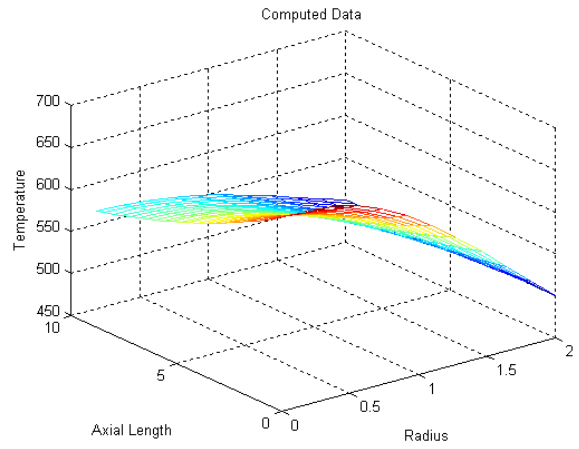

Fig. 10. Computed Data.

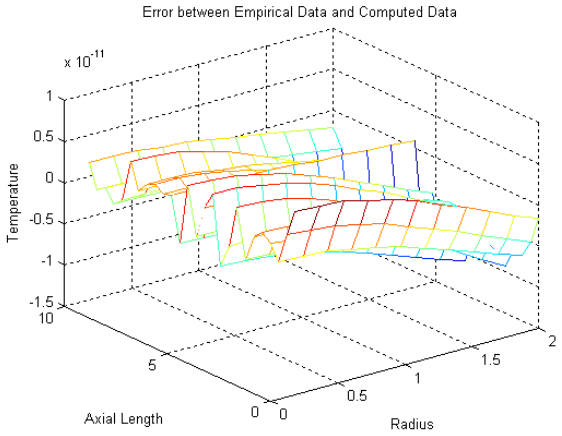

Fig. 11. Error between empirical data and computed data.

3.3.2.2. Case II. (NOISY ENVIRONMENT)

The results are shown in Figs. 12~ 18. Fig. 12 and Fig.18 show that the coefficient vectors are not smooth any more. Therefore, the semi-group channel should be used to smoothen the coefficient vector, prior to estimating the temperature.

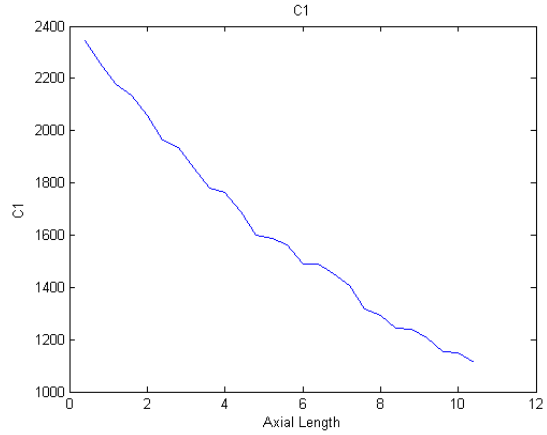

Fig.12. Coefficient Vector c_1.

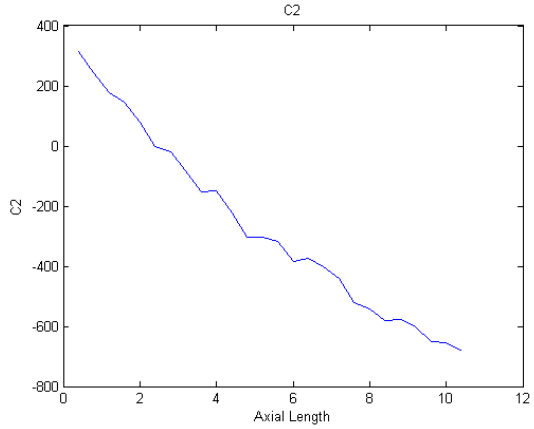

Fig. 13. Coefficient Vector c_2.

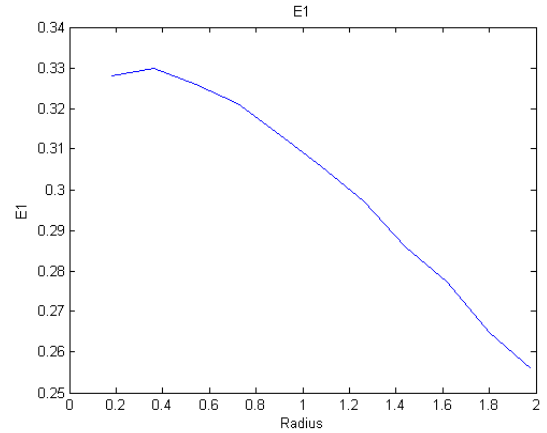

Fig. 14. Basis Vector e_1.

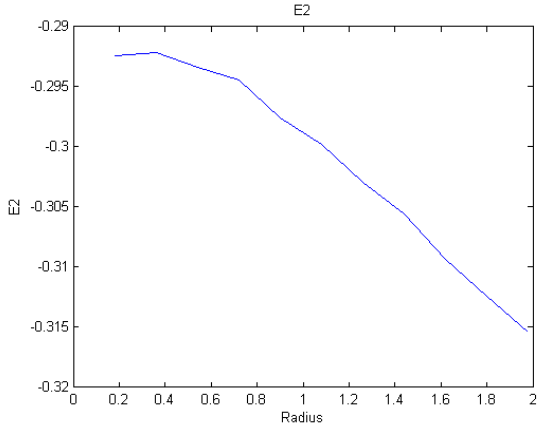

Fig. 15. Basis Vector e_2.

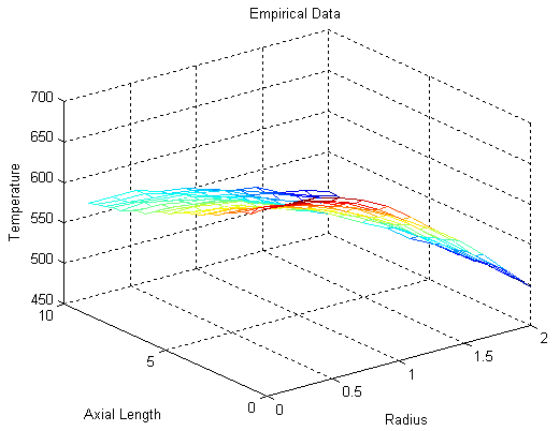

Fig. 16. Empirical Data.

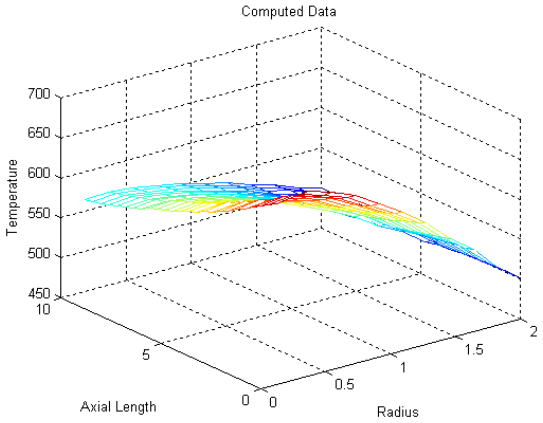

Fig. 17. Computed Data.

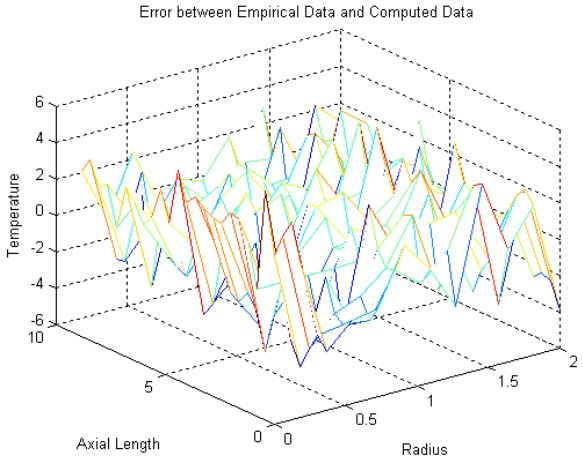

Fig. 18. Error between empirical data and computed data.

3.3.3 Estimation. (Derivation of analytic expression for temperature model)

3.3.3.1 Case I. (NOISE-FREE ENVIRONMENT)

To estimate the temperature, we first derive numerical expressions for the coefficient vectors and basis vectors. We get the following equations for c_1 and c_2:

$$c_1(z) = -0.2z^3 + 9.1z^2 - 2e^{0.02}z + 2.4e^{0.03} \quad (1)$$

$$c_2(z) = -0.16z^3 + 7.4z^2 - 1.6e^{0.02}z + 3.4e^{0.02} \quad (2)$$

In addition, we have the following equations for the basis vectors e_1, e_2.

$$e_1(r) = 0.0086r^3 - 0.045r^2 + 0.019r + 0.33 \quad (3)$$

$$e_2(r) = 0.0026r^3 - 0.014r^2 + 0.0058r - 0.29 \quad (4)$$

Consequently, we can estimate the temperatures at any point in the continuum (in the interior of the boiler furnace) by expanding the following function:

$T(z,r)= c_1[z]*e_1[r]+c_2[z]*e_2[r]$ using the above expressions. Fig. 19 shows the result of this estimation.

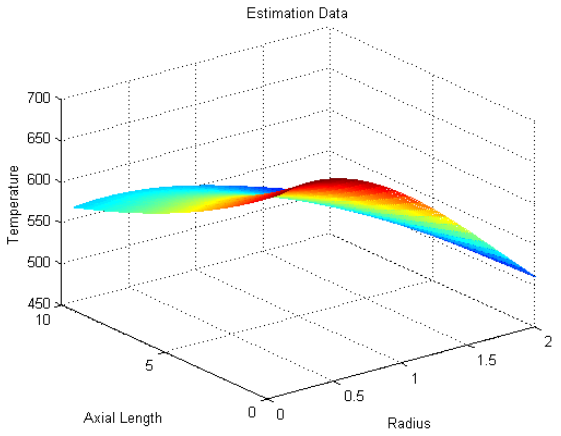

Fig.19. Estimation Data.

3.3.3.2 Case II. (NOISY ENVIRONMENT).

In this case, we have rough coefficient vector characteristics. Therefore, we use the semi-group channel to perform smoothing. Fig. 20 and Fig. 21 show the smoothened coefficient vector c_1 and c_2. Fig. 22 and Fig. 23 show the basis vector and the expressions. Notice that the basis vectors need not be smooth, since there is no associated semigroup property they must satisfy. From the smoothened coefficient vector, we can get numerical expressions of each coefficient vector. Equation (5) and (6) are the coefficient vector expressions and equation (7) and (8) are the basis vector expressions.

$$c_1(z) = -9.1e^{-0.06}z^3 + 0.00077z^2 - 0.019z + 0.24 \quad (5)$$

$$c_2(z) = -1.9e^{-0.05}z^3 + 0.00083z^2 - 0.016z + 0.032 \quad (6)$$

$$e_1(r) = 0.0078r^6 - 0.045r^5 + 0.093r^4 - 0.065r^3 - 0.039r^2 + 0.033r + 0.32 \quad (7)$$

$$e_2(r) = 0.0092r^6 - 0.056r^5 + 0.13r^4 - 0.15r^3 + 0.079r^2 - 0.021r - 0.29 \quad (8)$$

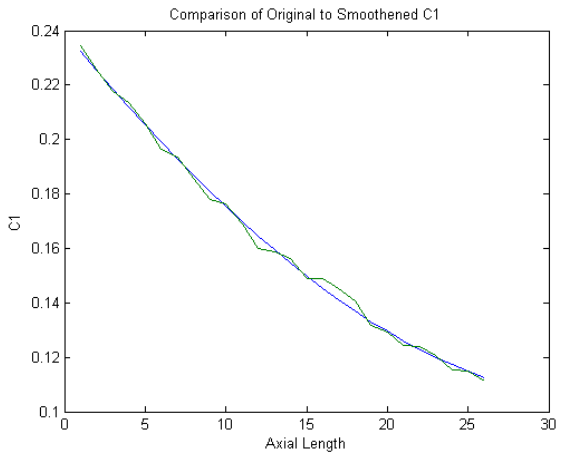

Fig. 20. Smoothened c_1.

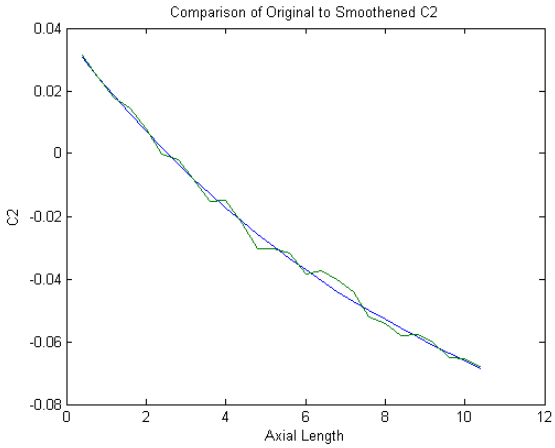

Fig. 21. Smoothened c_2.

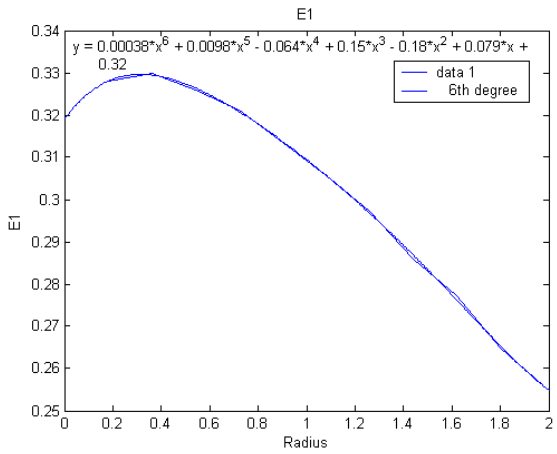

Fig. 22. Numerical Expression for e_1.

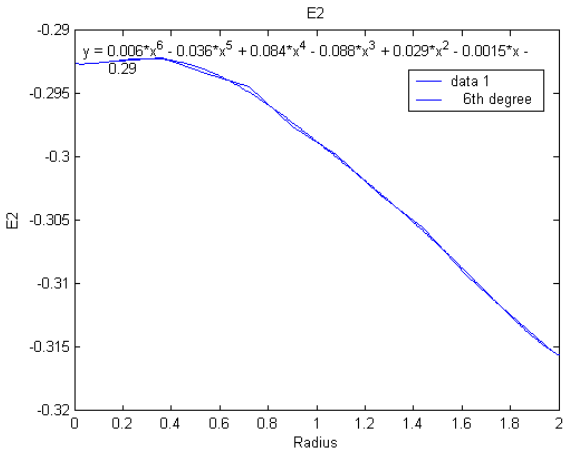

Fig. 23. Numerical Expression for e_2.

Using above results, we still can estimate the temperature using the equation $T(z,r)=c_1[z]*e_1[r]+c_2[z]*e_2[r]$ as in case I. Fig. 24 shows the result of this estimation. (Notice that the noise has been removed and, more importantly, that the estimation applies to the entire continuum defined by the interior of the furnace.)

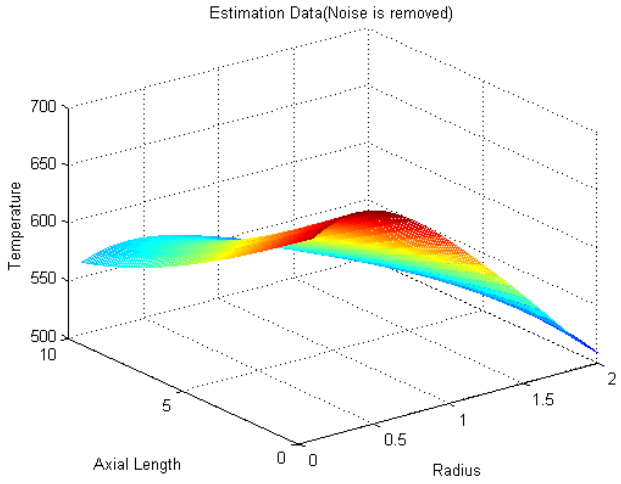

Fig.24. Estimation Data.

3.3.4 Extrapolation.

Extrapolation can only begin after smoothing has been accomplished, which has the effect of removing the noise. Therefore, only one case will be considered. Extrapolation occurs on the interval from $z = 10$ to $z = 13.3$, by making use of the functionality derived on the interval from $z = 0$ to $z = 10$. Figs. 25, 26 and 27 illustrate the strong weight convergence which is a necessary condition for extrapolation. Figs. 28 and 29 illustrate the results of extrapolation for each component of the $C(z)$ vector.

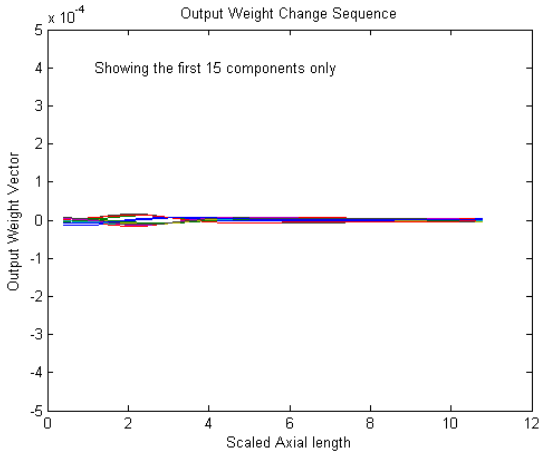

Fig. 25. Output Weight Vector Change.

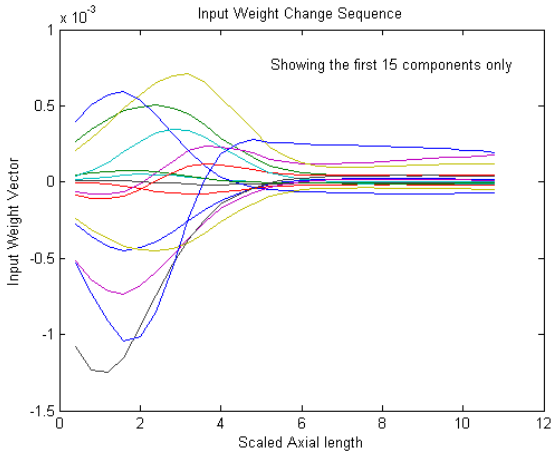

Fig. 26. Input Weight Vector Change.

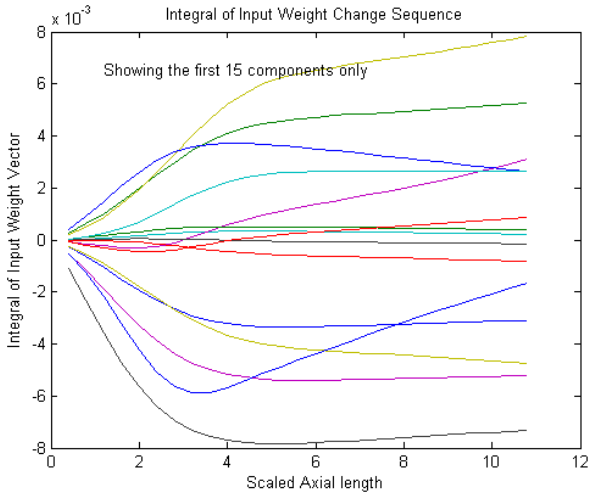

Fig. 27. Integral of Input Weight Vector Change.

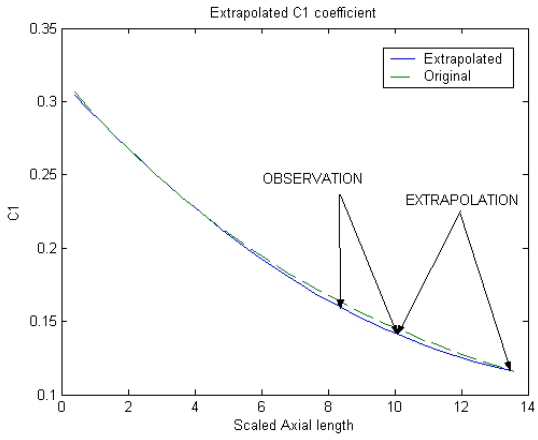

Fig. 28. Extrapolated C1 Coefficient.

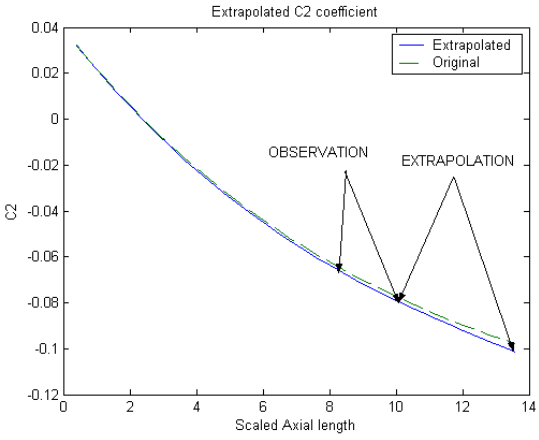

Fig. 29. Extrapolated C2 Coefficient.

The same procedure which was used in section 3.3 to develop an analytic expression for both $C(z)$ and $E(r)$ (and therefore for $T(z,r)=c_1[z]*e_1[r]+c_2[z]*e_2[r]$) for the region for which there was data ($z = 0$ to $z = 10$), can be applied to develop a continuum model for the extrapolated region.

3.4 Conclusions

In this research, we introduced a new estimation method using intelligent technique based on a neural network implementation of the semi-group property. From the results, we show that the proposed estimation method works well even in the presence of noise. This procedure was used both for interpolation (to develop a continuum model in the region from $z = 0$ to $z = 10$) and also for extrapolation (to develop a continuum model for the region from $z = 10$ to $z = 13.3$). Additionally, the method can be applied to parameter estimation.

3.5 Future Work Plan

In the next year, we will implement the project according to the working plan as described in the original proposal.

3.6 References

[1] Elman.J., "Finding Structure in Time", *Journal of Cognitive Science*, Vol. 14, pp. 179 - 211, (1990).

[2] Eckert, E.R.G., Drake R.M., *Analysis of Heat and Mass Transfer*, McGraw-Hill, New York, pp. 333 - 342, (1972).

[3] K. Y. Lee., S. N. Chow and R. O. Barr, "On the control of discrete-time distributed parameter systems", SIAM Journal on Control, Vol. 10, No. 2, pp. 361-376, (1972).

[4] K. Y. Lee and R. O. Barr, "Sampled-data optimization in distributed parameter system", IEEE transactions on automatic control, AC-17, pp. 806-809, (1972).

[5] K. Y. Lee and R. O. Barr, "Optimal sampled-data regulators of distributed parameter systems", Proc. IEEE Conference on Decision and Control, pp. 607-711, (1971).

[6] K. Y. Lee., "Optimal estimation of operator-valued stochastic processes and applications to distributed parameter systems", Proc. IEEE Conference on Decision and Control, pp. 94-98, (1972).

[7] K. Y. Lee, "Optimal estimation of first order distributed systems: multiplicity and martingale research," Proc. Joint Automatic Control Conference, pp. 634-636, (1976).

[8] K. Y. Lee, "On the estimation of distributed systems with uncertain parameters", Proc. IEEE Conference on Decision and Control, pp. 1128A-1128C, (1976).

[9] R.Jacobs and M. Jordan, “A Competitive Modular Connectionist Architecture”, Advances in Neural Information Processing Systems, Vol. 3, p. 767-773, (1991).

[10] Eckert, E.R.G., Drake R.M., Analysis of Heat and Mass Transfer, McGraw-Hill, New York, pp. 333 - 342, (1972).

RELATED TECHNICAL PUBLICATIONS

Refereed Journal Papers:

1. Kun-wook Chung, Sungwon Kim, and Shizhuo Yin, “Design of a highly nonlinear dispersion-shited fiber with a small effective area by use of the beam propagation method with the Gaussian approximation method,” Optics Letters., Vol. 28, pp. 2031-2033 (2003).

2. Shizhuo Yin, Youwei Fu, and Sung-Hyun Nam, “An experimental investigation on electrically controlled wavelength selective holographic switch,” Optics Memory and Neural Networks, No. 2, pp. 131-138, 2003.

3. Wei-Hung Su, Hongyu Liu, Karl Reichard, Shizhuo Yin, and Francis Yu, “Fabrication of digital sinusoidal gratings and precisely controlled flats and their applications to highly accurate projected fringe profilometory,” Optical Engineering, Vol. 42 (6), pp. 1730-1740, (2003).

4. Shizhuo Yin, Purwadi Purwosumarto, Weihong Su, and Claire Luo, Y. Sheng "An athermal hitless, tunable add-drop module with inherently integrated power controller," Microwave and Optics Technology Letter, Vol. 36, pp. 297-300 (2003).

5. Shizhuo Yin, Purwadi Purwosumarto, Zhuanyun Guo, and Fang Luo, "A polarization independent athermal electro-optic bulk modulator uisng a unique sandwich configuration," Microwave and Optics Technology Letter Vol. 36, pp. 157-160 (2003).

6. Shizhuo Yin, Purwadi Purwosumarto, Weihung Su, and Claire Luo, "A highly integrable, compact, reliable, and low WDL fiber optic tap coupler," Microwave and Optics Technology Letter, Vol. 36, pp. 166-170 (2003).

Refereed Conference Proceedings

1. Shizhuo Yin, Sung-Hyun Nam, Jesus Chavez, Chun Zhan, and Claire Luo, “Innovative long period gratings: principles and applications,” SPIE 5206, pp.30-44, San Diego, CA, Aug., 2003 (**invited paper**)

2. Yin, Zhiwen Liu, Iam-Choon Khoo, Kun-Wook Chung, and Yi Yang, "Tunable photonic crystal fibers and their applications," American Ceramic Society Meeting on Optical Waveguides: Unconventional Approaches and Applications, Oct, Corning, NY, 2003.

3. Sung Hyun Nam, Wei-Hung Su, Jesus Chavez, and Shizhuo Yin, "A unique all-optic switch based on an innovatively designed liquid crystal waveguide," SPIE 5206, pp.290-298,, San Diego, CA, Aug., 2003.

REVIEW MEETING

We attended the annual review meeting held on June 3-4, 2003 in Pittsburgh, PA.